

Breathers in a Discrete Nonlinear Schrödinger type Model : Exact Stability Results.

Avijit Lahiri¹, Subhendu Panda² and Tarun K. Roy²

¹Dept of Physics, Vidyasagar Evening College, Kolkata 700 006, INDIA

²Saha Institute of Nuclear Physics, 1/AF, Bidhannagar, Kolkata 700 064, INDIA

Exact stability analysis of 1-site breathers in an NLS type model (ref. [4], see below) indicates destabilisation through a growth rate becoming positive as a stability border is crossed, while above a critical spatial decay rate (λ_c) the breather is always unstable. Similar analysis on 2-site breathers with phase difference π (see below) indicates destabilisation through *Krein collision* of a pair of growth rates. All eigenmodes can be exactly calculated and conform to numerical estimates.

PACS number(s): 05.45.-a, 63.20.Pw, 63.20.Ry

The question of dynamical stability of discrete breathers has been addressed in the literature and a number of useful results are now known. The stability of a monochromatic breather depends on the eigenvalues of a symplectic matrix, the so called Floquet matrix. Aubry [1] introduced a novel extension to the concept of the Floquet matrix, thereby greatly simplifying the task of computing the Floquet multipliers and of looking for the onset of instability. In particular, he established that, one-site breathers sufficiently close to the ‘anti-integrable’ limit are dynamically stable. However, few exact results relating to the multipliers and the associated eigenmodes are known ([2], [3]; see references therein for a background to the problem) notably because the breather solutions around which the linearisation is to be performed are themselves obtained numerically, even though with high precision. In this context it is useful to have models that admit of *exact* breather solutions as also exact stability results. In [4] we introduced a number of piecewise smooth (PWS) models including a nonlinear Schrödinger type one and worked out exact one-site breather solutions where one of the sites is excited to a value above a *threshold* while all other sites remain below the threshold (we denote these as respectively *high* and *low*). In the present paper we work out exact stability results for these breathers as also for *2-site* breathers where two sites with an arbitrary intervening gap are *high* while all other sites are *low*. While the destabilisation of 1-site breathers always occur through the growth rate of a mode becoming positive, the 2-site breathers get destabilised through a *Krein collision* of the growth rates (see below). More precisely, the PWS Schrödinger type model introduced in [4] is

$$i \frac{d\psi_n}{dt} + V(\psi_{n+1} + \psi_{n-1}) = \gamma \psi_n f(\psi_n), (n = 0, \pm 1, \dots) \quad (1)$$

$$f(z) = -(1 - a/|z|)\Theta(|z| - a), \quad (2)$$

where $a(> 0)$, $V(> 0)$, γ are appropriate constants and Θ denotes the Heaviside step function. We scale the nearest neighbour coupling strength and the threshold parameter to $V = 1$, $a = 1$. Fig.1 compares $f(z)$ of (2) with the more usual form $f(z) = -|z|^2$ of the discrete

non-linear Schrödinger equation. The one-site breather solution centred at $n = 0$ is then

$$\bar{\psi}_n = \bar{\phi}_n e^{-i\omega t}, \quad (3)$$

$$\bar{\phi}_n = \frac{\gamma \lambda^{|n|}}{\gamma + \lambda - 1/\lambda}. \quad (4)$$

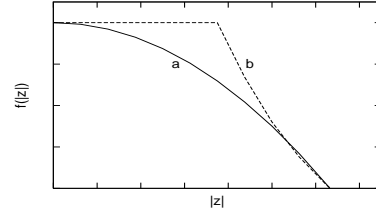


FIG. 1. Comparison of function $f(z)$ (a) of the usual form $f(z) = -|z|^2$ with (b) of Eq.(2).

The spatial decay rate λ ($|\lambda| < 1$) and the breather frequency ω satisfy

$$|\omega| > 2, \quad \omega = -(\lambda + 1/\lambda), \quad \omega\gamma < 0, \quad |\gamma| > 1 + \frac{1}{|\lambda|}, \quad (5)$$

(note: Equations (10), (11) in [4] expressing the above relations contained errors due to oversight, which we regret). We distinguish between breathers of *type A* ($\lambda > 0, \omega < -2$) and *type B* ($\lambda < 0, \omega > 2$), referring to the former in presenting our results below (results for type B are obtained analogously). The overbar in (3),(4) is used to distinguish the breather solution from neighbouring perturbed solutions (see below).

We consider these perturbations in the ‘rotating frame’ in the form

$$\psi_n = (\bar{\phi}_n + u_n(t))e^{-i\omega t}. \quad (6)$$

Splitting u_n into real and imaginary parts, $u_n = x_n + iy_n$, one observes that the time variations of x_n , y_n are obtained from the Hamiltonian

$$H = \sum_n \left\{ (x_{n+1}x_n + y_{n+1}y_n) + \frac{\omega}{2}(x_n^2 + y_n^2) \right\} + \frac{\gamma}{2} \{ x_0^2 + y_0^2 (1 - \frac{1}{b}) \},$$

where $b = \frac{\gamma}{\gamma + \lambda - \frac{1}{\lambda}}$. Eigenvalues of the matrix L determining the evolution of the x_n 's and y_n 's will be termed *growth rates* (we denote a typical growth rate by the symbol p) while a more convenient approach in the present context is to eliminate the y_n 's or x_n 's, arriving at

$$\ddot{X} = AX, \quad \ddot{Y} = A^T Y \quad (\mu \neq 0), \quad (7)$$

where we define $X = (\dots\dots x_{-2}, x_{-1}, x_0, x_1, x_2, \dots\dots)^T$, $Y = (\dots\dots y_{-2}, y_{-1}, y_0, y_1, y_2, \dots\dots)^T$, and A is a banded matrix with elements a_{mn} ($-\infty < m, n < \infty$) differing from zero only when $|m - n| \leq 2$:

$$\begin{aligned} a_{0,0} &= 2(\gamma\lambda - 2 - \lambda^2), \\ a_{0,1} &= a_{0,-1} = 3\lambda + 1/\lambda, \\ a_{1,0} &= a_{-1,0} = 2\lambda + 2/\lambda - \gamma, \\ a_{n,n} &= -(\lambda^2 + 1/\lambda^2 + 4), \quad (n \neq 0), \\ a_{n,n+1} &= a_{n+1,n} = 2(\lambda + 1/\lambda), \quad (n \neq 0, -1), \\ a_{n,n+2} &= a_{n+2,n} = -1. \end{aligned}$$

The eigenvalues (μ) of A are related to growth rates (p) as $\mu = p^2$. The spectrum of eigenvalues μ and the corresponding eigenmodes can all be worked out exactly for any given parameter values λ , γ satisfying (5). There exists a band of eigenvalues $-(\omega - 2)^2 < \mu < -(\omega + 2)^2$ with *extended* eigenmodes, there being a *symmetric* and an *antisymmetric* eigenmode associated with each eigenvalue. Additionally, there exists a single *localised* symmetric eigenmode for $\gamma > \gamma_1(\lambda)$ where

$$\gamma_1(\lambda) = \frac{(\lambda - \frac{1}{\lambda})\sqrt{((\lambda + \frac{1}{\lambda})^2 - 2(\lambda + \frac{1}{\lambda}))}}{(\lambda - \frac{1}{\lambda}) + \sqrt{((\lambda + \frac{1}{\lambda})^2 - 2(\lambda + \frac{1}{\lambda}))}}.$$

For any given λ , γ_1 is thus the *threshold* for the localised mode: for $\gamma < \gamma_1$ there is no localised mode and the band edges are empty, while for $\gamma = \gamma_1$ an eigenmode appears at the band-edge, and dissociates from the band as the localised mode for $\gamma > \gamma_1$. One notes in this context that there always exists a trivial eigenmode $\mu = 0$ with $x_n = 0$, $y_n \propto \phi_n$, which is to be distinguished from the eigenvectors of A , A^T with $\mu = 0$, the latter corresponding to a spurious mode in the present context. While a typical localised eigenvector of A is of the form

$$x_n = \alpha\chi_1^{|n|} + \beta\chi_2^{|n|},$$

where the spatial decay rates χ_1 , χ_2 (each of modulus < 1) as also the ratio α/β can be obtained exactly, the eigenvector corresponding to $\mu = 0$ looks like

$$x_n = (\alpha + \beta|n|)\lambda^{|n|}.$$

The growth rates for the localised mode are imaginary ($p = \pm i\sqrt{|\mu|}$) so long as $\gamma_1(\lambda) < \gamma < \bar{\gamma}(\lambda)$ where the transition value $\bar{\gamma}$ can also be obtained exactly in the model:

$$\bar{\gamma}(\lambda) = \frac{(1 + 4\lambda^2 + \lambda^4)(1 - \lambda^2)}{2\lambda^3}.$$

As γ crosses $\bar{\gamma}$ from below, the isolated eigenvalue μ crosses $\mu = 0$ and becomes positive, giving rise to a positive growth rate ($p_+ = \sqrt{\mu}$; this is associated with a negative growth rate $p_- = -\sqrt{\mu}$, making up a pair) and implying destabilisation of the breather.

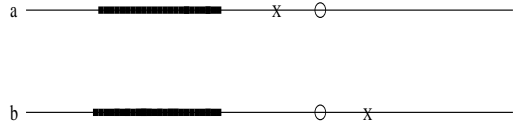


FIG. 2. Spectrum of eigenvalues of matrix A for (a) $\gamma_1(\lambda) < \gamma < \bar{\gamma}(\lambda)$ and (b) $\gamma > \bar{\gamma}(\lambda)$; cross denotes eigenvalue for the isolated localised mode while thick black line denotes the band; circle corresponds to $\mu = 0$.

Fig.2 depicts the disposition of eigenvalues on either side of the destabilisation, while

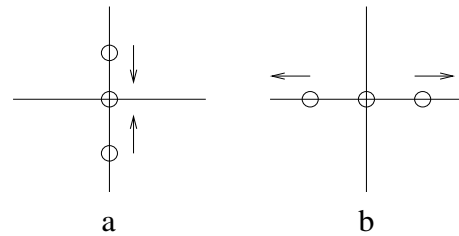


FIG. 3. Disposition of growth rates p in the complex plane with (a) $\gamma < \bar{\gamma}$ (b) $\gamma > \bar{\gamma}$

Fig.3 indicates how the disposition of growth rates in the complex plane changes across the destabilisation border.

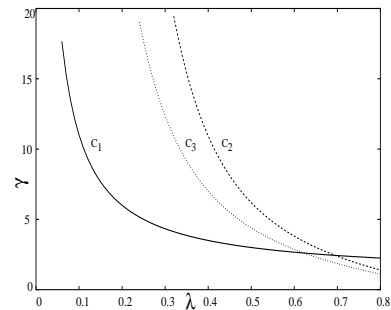


FIG. 4. Curves C_1 ($\gamma = \gamma_0(\lambda)$), C_2 ($\gamma = \bar{\gamma}(\lambda)$) and C_3 ($\gamma = \gamma_1(\lambda)$) in the $\lambda - \gamma$ plane; the point of intersection of C_1 and C_2 corresponds to $\lambda = \lambda_c \approx 0.6948$

Fig.4 depicts the $\lambda - \gamma$ parameter space for the model together with the curves C_1 ($\gamma = \gamma_0(\lambda) \equiv 1 + \frac{1}{\lambda}$), C_2 ($\gamma = \bar{\gamma}(\lambda)$), C_3 ($\gamma = \gamma_1(\lambda)$). The breather exists only for points lying above C_1 and is stable only for points lying below C_2 , *i.e.*, for (λ, γ) lying in between C_1 and C_2 the model admits of a stable breather solution. The curve C_3

gives the *threshold* for the localised mode. Interestingly, the model predicts the existence of a critical value (λ_c) of the spatial decay rate corresponding to the intersection of C_1 and C_2 ($\lambda_c \approx 0.6948$) so that the breathers with $\lambda > \lambda_c$ are unstable for all values of the strength of non-linearity γ ($> \gamma_0(\lambda)$). All these features resemble those of ‘internal’ or ‘breathing’ modes of DNLS breathers whose relevance has been emphasized in the literature ([5], [6]). However, the antisymmetric ‘pinning’ mode [6], known to exist for DNLS breathers, is marginal in the present PWS model ($\lambda = 1$, $\mu = 0$) and possesses a linear spatial growth.

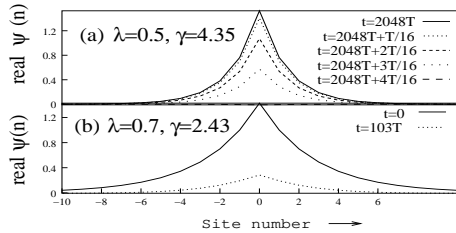


FIG. 5. Numerical integration following (1), (2) of an initial profile given by (4) at $t = 0$; (a) $\lambda = 0.5$, $\gamma = 4.35$, in between C_1 and C_3 of Fig.3 - profiles at values of t spanning a quarter of a period ($T/4$) starting from $2048T$; (b) $\lambda = 0.7$ (just beyond intersection of C_1 and C_2 in Fig.3), and $\gamma = 2.43 (> \gamma_0(\lambda))$.

We show in Fig.5a the temporal evolution according to Eqs. (1), (2) of a profile initially ($t=0$) coinciding with (3), with (λ, γ) in the region between C_1 and C_2 while Fig.5b shows the similar evolution for a breather with $\lambda > \lambda_c$, above C_1 . One notes that the breather in Fig. 5a performs stable oscillations while that in Fig. 5b breaks up within a short time, confirming our results. In this context see also Figs. 4,5 of [4].

The eigenmodes can be obtained exactly in the model. For instance, Fig.6 shows the localised eigenmode for $\lambda = 0.5$, $\gamma = 6$ calculated from the theory as compared with the eigenmode obtained numerically by diagonalising the matrix A .

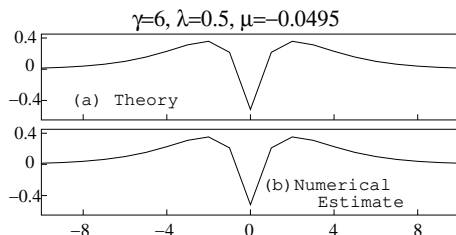


FIG. 6. Eigenmodes obtained (a) from exact analysis and (b) by diagonalising the matrix A

As we mentioned in [4], the PWS model (1), (2) is a veritable little ‘laboratory’ yielding exact breather solutions of a wide variety. For instance, one can construct

two-site breathers with various possible lengths of intervening gap N . One other feature of crucial relevance is the relative *phase* between the two sites. This relates to the fact that (4) admits of an arbitrary phase factor $e^{i\delta}$ that becomes relevant in 2-site or multisite breather solutions. Thus, considering a breather with two sites *high* (i.e., with $|\psi_n| > 1$) and all the other sites *low* ($|\psi_n| < 1$) with the *high* sites having opposite phases ($\delta = \pi$) one obtains a monochromatic breather solution of the form (3) with the breather profile $\bar{\phi}_n$ now given by

$$\begin{aligned} \bar{\phi}_n &= \frac{b}{1 - \lambda^N} (\lambda^n - \lambda^{N-n}) & (0 \leq n \leq N) \\ &= b\lambda^{-n} & (n < 0) \\ &= -b\lambda^{n-N} & (n > N), \end{aligned} \quad (8)$$

where $b = \frac{\gamma(1-\lambda^N)}{\gamma(1-\lambda^N) - (\lambda^{-1}-\lambda)}$ and λ , γ are to satisfy $\gamma > \frac{1+\lambda^{-1}}{1-\lambda^N}$. Here the two *high* sites have been chosen to be at $n = 0$ and $n = N$ for any given separation N . It is now easy to construct the stability matrix A of Eq.(7) and to obtain the spectrum of eigenvalues together with the exact eigenmodes. There is once again a band extending from $-(\omega - 2)^2$ to $-(\omega + 2)^2$ (recall that we are considering only type A breathers, with $\omega < -2$) containing extended eigenmodes, together with a number of isolated eigenvalues corresponding to localised modes. The latter appear above a certain *threshold* value of γ (for any given λ), and are now typically *four* in number of which one is the trivial eigenvalue $\mu = 0$ while the others lie in the range $-(\omega + 2)^2 < \mu < 0$. Ordering these as $\mu_1 < \mu_2 < \mu_3 < \mu_4 = 0$, the eigenmodes corresponding to μ_1 and μ_4 are *antisymmetric* (with respect to the sites $n = 0, N$) while the other two are *symmetric*. Fig.7 shows the four eigenmodes for $N = 8$, $\gamma = 4.9443$, $\lambda = 0.5$. For a given N , λ , as γ is made to increase from the threshold value, a boundary $\gamma_H(\lambda)$ is reached when μ_2 and μ_3 become coincident and then become complex. In terms of the growth rates p ($p = \pm\sqrt{\mu}$) there occurs a Krein collision of a quartet of growth rates on the imaginary axis and the subsequent splitting of the growth rates out of the complex plane, as depicted schematically in Fig.8.

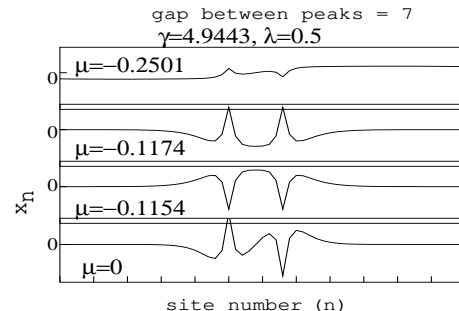


FIG. 7. Symmetric and antisymmetric localised eigenmodes for a 2-site breather.

In a model with sufficiently smooth $f(z)$ (ref. Eq.2) this leads to the *Hamiltonian Hopf bifurcation* ([7], see references therein; the Krein collision has been discussed in [1] in terms of the Floquet multipliers related to the breather solution - the latter are related to our eigenvalues (μ) and the corresponding growth rates (p) in a simple manner; there exists a large body of literature relating to Krein collision in symplectic mappings - see, *e.g.*, [8]). In the present context, the collision signifies a loss of stability. For instance, with $N = 8, \lambda = 0.5$, the model predicts a loss of stability of the two-site breather through a Krein collision at $\gamma_H \approx 4.9444$.

Fig.9 depicts the time evolution of an initial profile chosen in accordance with (8) with γ on either side of the collision: one notes that the breather indeed remains stable for $\gamma < \gamma_H$ and breaks up quickly for $\gamma > \gamma_H$.

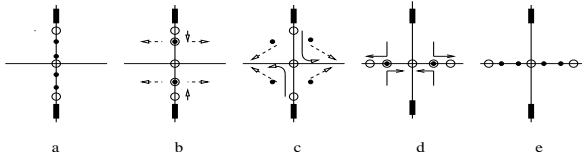


FIG. 8. Sequence of changes in the disposition of growth rates in the complex plane; thick black lines denote the band while the dots and circles correspond to localised modes; (a) before Krein collision ($\gamma < \gamma_H$; λ fixed), (b) Krein collision $\gamma = \gamma_H$, (c) a quartet of complex growth rates resulting from the Krein collision, and a pair of imaginary growth rates approaching collision at $p = 0$, (d) Krein collision ‘in the reverse’, (e) all four growth rates of localised modes real.

As mentioned above, in Fig.8 we depict the sequence of changes in the disposition of the growth rates p as γ is made to increase through γ_H for fixed λ . One observes that at some value $\tilde{\gamma} (> \gamma_H)$ of γ , the root μ becomes positive (this is similar to the crossing of a negative eigenvalue through the value zero at $\gamma = \tilde{\gamma}(\lambda)$) with μ_2, μ_3 remaining complex; subsequently at some value $\gamma = \gamma'_H$ the latter collide at a point on the positive real axis and move off in opposite directions - Krein collision ‘in the reverse’. In the present context of stability of the breathers, however, this reverse collision does not have a direct relevance since the breather, having become unstable at $\gamma = \gamma_H$ continues to remain unstable even at $\gamma = \tilde{\gamma}$ and $\gamma = \gamma'_H$. For large N , one finds that $\gamma_H, \tilde{\gamma}$ and γ'_H are all contained in a small interval around $\tilde{\gamma}$ as expected, since the two

high sites are then almost unaffected by each other, each essentially behaving like a one-site breather (3), (4). Interestingly, a 2-site breather with the two *high* sites *in phase* with each other can also be constructed in the model, but turns out to be always unstable.

The details of the calculations together with numerical and other results on breather stability will be presented elsewhere.

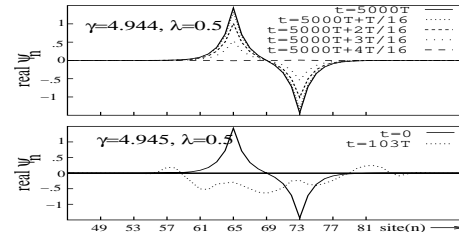


FIG. 9. Numerical integration following (1), (2) of an initial two-site breather profile given by (8): (a) $\gamma < \gamma_H(\lambda)$, (b) $\gamma > \gamma_H(\lambda)$.

-
- [1] S. Aubry, Physica D, 103 (1997) 201-250.
 - [2] S. Flach, and C. R. Willis, Phys. Rep. 295 (1998) 181-264.
 - [3] G. Kevrekedis, K. Ø. Rasmussen, A. R. Bishop, Phys. Rev. E61 (2000) 2006-2009.
 - [4] A. Lahiri, S. Panda, T. K. Roy, Phys. Rev. Lett. 84,(2000) 3570-3573.
 - [5] E. W. Laedke, O. Kluth, K. H. Spatschek, Phys. Rev E 54 (1996) 4299-4311
 - [6] M. Johansson, S. Aubry, Y. B. Gaididei, P. L. Christiansen, K. Ø. Rasmussen, Physica D 119 (1998) 115-124.
 - [7] A. Lahiri, M. Sinha Roy, Int. Jour. Nonlin. Mech., 36 (2001) 787-802.
 - [8] T.J. Bridges and J. E. furter, *Singularity Theory and Equivariant symplectic maps* ; Springer Verlag, Berlin, 1993.